ROYAL SOCIETY OF CHEMISTRY

PAPER

Check for updates

Guest-controlled polymorphism and exceptionally marked bi-stability in a spin crossover 3D porous amino-functionalized coordination polymer†

Alejandro Orellana-Silla,[a] Manuel Meneses-Sánchez,[a] Rubén Turo-Cortés, [ID][a] Víctor Rubio-Giménez, [ID]‡[b] Giel Arnauts,‡[b] M. Carmen Muñoz, [ID][c] Rob Ameloot, [ID][b] Carlos Bartual-Murgui [ID]*[a] and José Antonio Real [ID]*[a]

Functionalization of spin crossover (SCO) porous coordination polymers (PCPs) with hydrogen-bonding active groups is an efficient strategy for the study of multifunctional materials. Indeed, the interaction of guests with the host framework may improve the cooperativity of the SCO inducing eventual occurrence of bi-stability. However, comprehensive magneto-structural studies are still needed to understand the role of guests in the enhancement of the SCO properties. Here, we report the 3D Hofmann-type PCP {Fe^{II}(dpyan)[Au^{I}(CN)$_2$]$_2$}·guest (dpyan = 2,5-di(pyridin-4-yl)aniline; guest = ethanol (**1·EtOH**), methanol (**1·MeOH**), nitrobenzene (**1·NO$_2$Bz**), water/methanol (**1·H$_2$O·MeOH**)) where the amino functionalized dpyan ligand has been selected to induce host–guest interactions. Our X-ray diffraction studies reveal that the packing mode of **1·guest** is determined by the trapped guest yielding either orthorhombic (**1·NO$_2$Bz** and **1·H$_2$O·MeOH**) or monoclinic (**1·EtOH** and **1·MeOH**) phases differing by subtle distortions of the framework. The thermal dependence of the magnetic susceptibility shows that all derivatives present SCO properties modulated by the amount and nature of the encapsulated guest as well as by the crystal phase. The latter is clearly evidenced for the orthorhombic derivatives which, concomitantly with partial desorption of guest, transform into the monoclinic phase whose SCO behaviour is radically different to that of the original orthorhombic structure. As a relevant example, when **1·NO$_2$Bz** (orthorhombic) converts into **1·0.77NO$_2$Bz** (monoclinic), the SCO drastically changes from a non-hysteretic gradual spin transition to a cooperative SCO with a colossal hysteresis 105 K wide. These remarkable SCO properties have been interpreted relying on the obtained structural information.

Introduction

The spin crossover (SCO) phenomenon refers to the property exhibited by some octahedrally coordinated 3d^4–3d^7 transition metals of switching between two electronic configurations, as determined by the distribution of the valence electrons within the t$_{2g}$ and e$_g$ orbitals.[1] A paradigmatic example of this molecular event involves the Fe^{II} ion (3d^6) which, in an appropriate hexacoordinated coordination sphere (usually of the type Fe^{II}N$_6$), can be controllably, reversibly, and detectably interconverted between the low spin (LS, e$_g^6$, $S = 0$, diamagnetic) and the high spin (HS, e$_g^4$t$_{2g}^2$, $S = 2$, paramagnetic) states through the application of external stimuli.[2] Importantly, resulting from their different electronic configurations, the interconversion between both states involves changes in the structure, and magnetic, optical and dielectric properties of the complex. This coupling between external perturbation and physical property modification places the SCO materials as promising candidates for the fabrication of spintronic devices.[3]

In the solid state, the change of the spin state is governed by the electron–phonon coupling between the switching metallic centres. Therefore, their degree of interaction will determine the efficiency with which the spin change is transmitted. Considering a thermally induced SCO, when the metallic centres are strongly bonded (*e.g.* by coordination and/or covalent bonds), the system will exhibit high cooperativity featuring

[a] Departamento de Química Inorgánica, Instituto de Ciencia Molecular (ICMol), Universitat de València, Catedrático José Beltrán Martínez, 2, 46980 Paterna, Spain. E-mail: carlos.bartual@uv.es, jose.a.real@uv.es

[b] Centre for Membrane Separations, Adsorption, Catalysis and Spectroscopy (cMACS), Katholieke Universiteit Leuven, Celestijnenlaan 200F, 3001 Leuven, Belgium

[c] Departamento de Física Aplicada, Universitat Politècnica de València, Camino de Vera s/n, 46022 Valencia, Spain

† Electronic supplementary information (ESI) available: Synthesis and characterization of samples, experimental and instrumental details. CCDC 2277962–2277967. For ESI and crystallographic data in CIF or other electronic format see DOI: https://doi.org/10.1039/d3tc02363j

‡ These authors contributed equally to this work.

an abrupt change of the physical properties. Indeed, this thermally-driven cooperative SCO can occasionally exhibit a hysteresis effect which confers bi-stability (i.e. memory effect)[4] to the material, a very sought after property for applications in solid-state memories and actuators.[5–9]

A quite appealing archetypal structure for obtaining SCO compounds with highly cooperative and hysteretic profiles are the 3D Hofmann-type porous coordination polymers (PCPs) with general formula {Fe^{II}(L)[M^{I}(CN)$_2$]$_2$}·guest (M = Au, Ag).[10] In this structure, formed by doubly interpenetrated networks, the Fe^{II} ions are strongly connected, equatorially, through linear dicyanometallate units and, axially, by organic L molecules (typically bis-monodentate pyridine-type ligands). A very interesting feature presented by this type of compounds is that the SCO properties are affected by host–guest interactions which in turn may be tunned through the rational selection of specific guests and the functionalization of the L pillar ligands. Indeed, overall, the presence of a guest generally improves the cooperativity of the spin transitions inducing the occurrence of thermal hysteresis.[11–17] However, although it is well stablished that host–guest interactions and guest-induced internal pressure are behind the emergence of cooperative and hysteretic effects,[18–22] the lack of structural information prevents a deeper understanding of bi-stability. In this context, the occurrence of polymorphism can eventually provide insight about the magneto-structural correlations since it permits to directly compare the SCO properties of different structural phases of a given compound.[23]

Here, we present the 3D Hofmann-type PCP {Fe^{II}(dpyan)[Au^{I}(CN)$_2$]$_2$}·guest (**1·guest**, dpyan = 2,5-di(pyridin-4-yl)aniline) whose amino functionalized pillaring dpyan ligand (Scheme 1) has been intentionally selected to promote the occurrence of host–guest interactions. Indeed, this compound crystallizes with different guest molecules depending on the solvents used during the synthesis (guest = ethanol (**1·EtOH**), methanol (**1·MeOH**), nitrobenzene (**1·NO$_2$Bz**), water/methanol (**1·H$_2$O·MeOH**)). Our structural data have revealed that the packing mode of **1·guest** is determined by the nature of the trapped guest yielding either orthorhombic (**1·NO$_2$Bz** and **1·H$_2$O·MeOH**) or monoclinic (**1·EtOH** and **1·MeOH**) phases
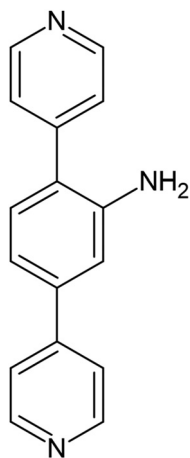
Scheme 1 Structure of ligand dpyan (2,5-di(pyridin-4-yl)aniline) used in this work.

through subtle distortions of the framework. Although the thermal dependence of the magnetic susceptibility shows that all derivatives present spin transitions, it has been found that their characteristics are governed by both the network packing and the nature of the trapped guest. This is clearly showcased for the orthorhombic derivatives which, concomitantly to the partial desorption of guest, transform into the monoclinic phase whose SCO behaviour is radically different to that of the original orthorhombic structure. As a relevant example, when **1·NO$_2$Bz** (orthorhombic) converts into **1·0.77NO$_2$Bz** (monoclinic), the thermally induced switching properties drastically change from a gradual non-hysteretic spin transition to a cooperative SCO displaying a colossal hysteresis width of 105 K. These remarkable SCO properties have been interpreted by relying on the obtained structural information.

Results

Synthesis and chemical characterization

All compounds were obtained as similar yellow plate-shaped single crystals through slow liquid–liquid diffusions of Fe(BF$_4$)$_2$· 6H$_2$O (or FeCl$_2$·4H$_2$O), dpyan and K[Au(CN)$_2$] solutions giving rise, depending on the used solvents, to different solvates of compound {Fe(dpyan)[Au(CN)$_2$]$_2$}·guest (**1·guest**) (see Experimental Section in ESI† for the synthesis details). Whereas single crystals of **1·MeOH** and **1·EtOH** are produced in pure methanol and ethanol solutions, respectively, crystals of **1·H$_2$O·MeOH** are obtained in mixed water/methanol solutions. Besides, crystals of the compound **1·NO$_2$Bz** are achieved in a nitrobenzene/ methanol diffusion medium.

The rapid loss of crystallinity observed for the as-synthesized crystals once removed from the mother liquor suggests a spontaneous desorption of the guest solvents. However, the thermogravimetric analysis (TGA), carried out for each solvate, indicates that a certain amount of guest is retained after exposing the crystals to air. Indeed, the resulting TGAs are consistent with the presence of ca. 0.5, 1.5, and 1 molecule of methanol, ethanol and nitrobenzene per Fe^{II} ion which are released within the 310–370 K (**1·MeOH**), 345–410 (**1·EtOH**), and 390–550 K (**1·NO$_2$Bz**) temperature range (Fig. S1, ESI†), respectively. For **1·H$_2$O·MeOH**, we performed mass spectrometry (MS) coupled with TGA to estimate if the remaining molecules of guest are either water or methanol. The results reveal a 2% of mass loss within the 300–400 K temperature range where the mass spectrum signals at 17 and 31 m/z confirm the retention of both water and methanol (Fig. S2, ESI†). This mass loss is far from the 5% expected for a 1 : 1 (H$_2$O : MeOH) stoichiometry inferred by crystallography (see below) indicating a clear partial solvent loss. When the same sample is measured after several weeks exposed to air, the recorded mass loss increases up to 3%. This fact, together with the observed larger relative amount of water with respect to methanol suggests a progressive adsorption of water from the humidity of air.

Given the lability of the guests in compounds **1·MeOH**, **1·EtOH** and **1·H$_2$O·MeOH**, the solvent free counterpart **1·ø** can be easily obtained through a mild thermal treatment at

13906 | J. Mater. Chem. C, 2023, **11**, 13905–13916

This journal is © The Royal Society of Chemistry 2023

400 K for 10 minutes. In contrast, because of its higher temperature of desorption, the guest molecules of nitrobenzene are only partially removed at 400 K. Thus, as observed by TGA, different samples with varying nitrobenzene contents (**1·0.77NO₂Bz**, **1·0.60NO₂Bz** and **1·0.34NO₂Bz**) were obtained after heating at 400 K during 20, 120 and 480 minutes, respectively, as verified by TGA (Fig. S3, ESI†). Treating the sample at a higher temperature (473 K) for 1 h was required to obtain the solvent free **1·ø** compound from **1·NO₂Bz**.

Aiming at investigating the susceptibility to re-adsorb water from the air moisture, a TGA was carried out on two samples of **1·ø** which were previously exposed to air overnight and for three days (Fig. S4, ESI†), respectively. The results indicate the loss of around 0.6 and 1.5% of mass, within the 300–400 K temperature range consistent with a gradual recovering of 0.3 and 0.7 molecules of water per Fe^{II} ion, respectively.

Single crystal X-ray diffraction

The structures of **1·NO₂Bz**, **1·H₂O·MeOH** and **1·EtOH** were determined at different temperatures (see below) through single crystal X-ray diffraction (SCRXD). Tables S1–S4 (ESI†) contain the crystallographic data including selected distances and angles of each compound. **1·NO₂Bz** and **1·H₂O·MeOH** are isomorphous (orthorhombic phase) and their structures will be described together. In contrast, the ethanol solvate presents a monoclinic phase and its structure will be described in a separated section. To prevent the desorption of the guest molecules and the consequent deterioration of the crystallinity, the crystals were directly transferred from the mother liquor, protected with perfluoropolyether cryo-oil, rapidly mounted on a cryoloop and placed in the diffractometer chamber below room temperature (260 K). Despite many attempts, the structure of **1·MeOH**, which is isostructural to **1·EtOH** (see below) could not be solved due to the rapid loss of crystallinity even surrounded by the oil. Similarly, the structure of **1·ø**, also isostructural to **1·EtOH**, was not achieved due to the collapse of the single crystals after desorption of the guests.

Structure of 1·NO₂Bz and 1·H₂O·MeOH (orthorhombic phase). At 250/260 K, the yellow crystals of **1·NO₂Bz**/**1·H₂O·MeOH** present the orthorhombic *Cmma* space group. The asymmetric unit of both compounds is formed by a unique pseudo-octahedral [$Fe^{II}N_6$] site coordinated equatorially by four equivalent [$Au(CN)_2$]⁻ units and axially by two equivalent dpyan ligands (Fig. 1a and b). The average bond lengths of the [FeN_6] octahedrons, ⟨Fe^{II}–N⟩$_{av}$, are 2.149 (**1·NO₂Bz**) and 2.148 Å (**1·H₂O·MeOH**) indicating that the Fe^{II} ions are in the HS state. Only three structural differences are observed when comparing the [FeN_6] environments of **1·NO₂Bz** and **1·H₂O·MeOH**: (i) despite both structures present positional disorder of the aniline moiety of the dpyan ligand, **1·H₂O·MeOH** exhibits an equivalent distribution of the NH₂ group disordered within the four available C atoms of the central ring and, in contrast, it only occupies two of them in **1·NO₂Bz**; (ii) while one of the two pyridine moieties bonded to the Fe^{II} centre displays positional disorder in **1·H₂O·MeOH**, no disorder is observed on the pyridines of **1·NO₂Bz**; (iii) the Au1–N1–Fe1 angle is larger for **1·NO₂Bz** (171.1°) than for
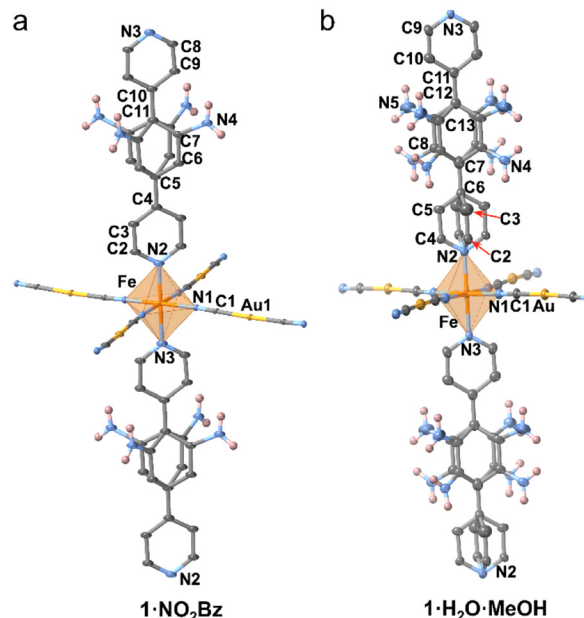
Fig. 1 Fragment of the crystal structures of (a) **1·NO₂Bz** and (b) **1·H₂O·MeOH** showing the corresponding atom numbering of the asymmetric unit cells.

1·H₂O·MeOH (165.8). As discussed below, all these structural differences seem to be related to the influence of the different size and nature of the trapped guests (*i.e.* water/methanol *vs.* nitrobenzene).

Both equatorial [$Au(CN)_2$]⁻ and axial dpyan units act as bridging ditopic ligands, thereby forming an extended 3D network (Fig. 2a). The high porosity exhibited by this network permits the interpenetration of an identical network stabilized by strong aurophilic interactions [Au···Au = 3.122 Å (**1·NO₂Bz**) and 3.154 Å (**1·H₂O·MeOH**) at 250 and 260 K, respectively], in such a manner that the apical dpyan ligands of one of them pass through the centroid of the {$Fe_4[Au(CN)_2]_4$} windows of the other (Fig. 2b and c). Despite the interpenetration, there is still enough void space to host guest molecules. In the case of **1·H₂O·MeOH**, the position of the methanol and water guests are clearly identified in the pores (Fig. 2d). The methanol molecule, located in the vicinity of the NH₂ group, is stabilized through a strong H₂N···HOCH₃ hydrogen bond [(d(N···O) = 2.655 Å)]. Besides, the methanol molecule interacts with one of water (O_{MeOH}···O_{water} = 3.143 Å), hence forming molecular chains stabilized through much weaker H-bonds that parallelly spread along the 1D channels of the network. In contrast, the nitrobenzene molecules in **1·NO₂Bz** are too disordered to identify their exact location. However, the electronic density found within the pores suggests that the position of the guests is not equivalent to that found for methanol and water in **1·H₂O·MeOH**. Instead, the electronic residue of the nitrobenzene molecules is homogenously distributed within the 1D pores rather than situated in the proximity of the NH₂ groups as observed in **1·H₂O·MeOH** (Fig. S5, ESI†). This is likely the reason for the lack of NH₂ groups pointing at the central part of the pores of **1·NO₂Bz**, as this space is required to

This journal is © The Royal Society of Chemistry 2023

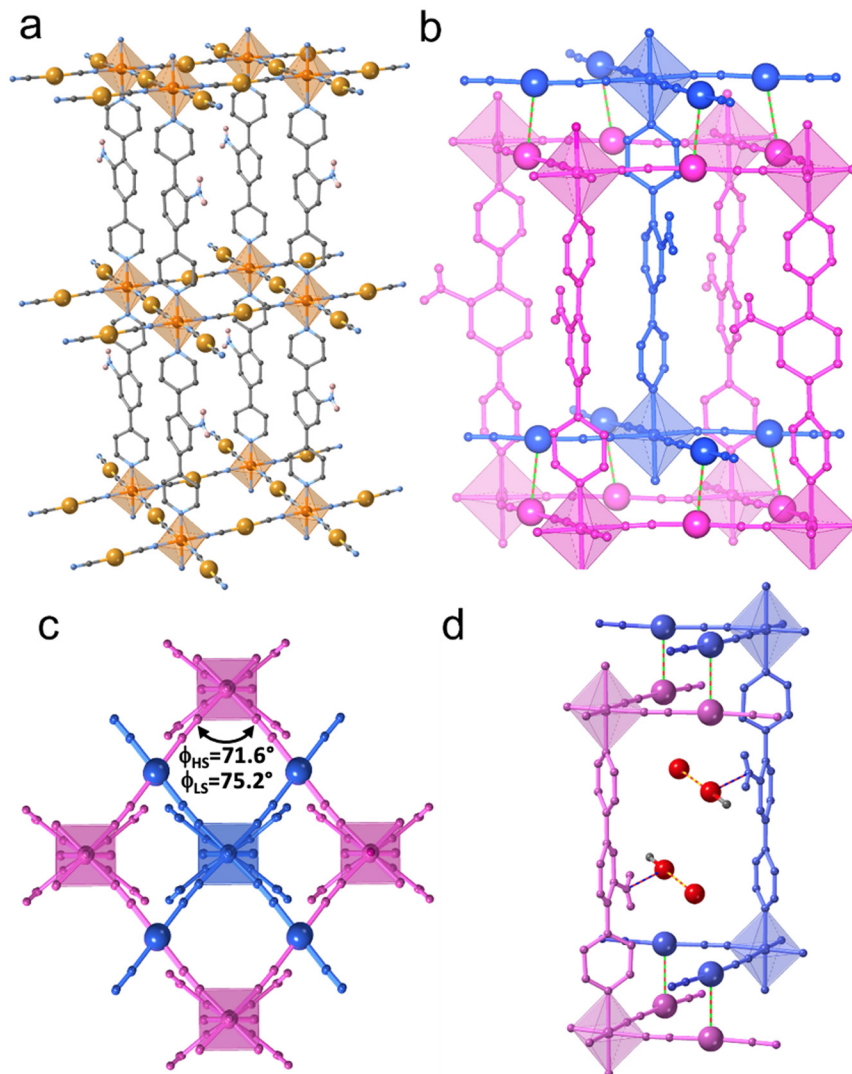*J. Mater. Chem. C*, 2023, **11**, 13905–13916 | **13907**

Fig. 2 (a) Perspective view of one of the two interpenetrated 3D networks of **1·H₂O·MeOH**. (b) Side and (c) top view showing the two interpenetrated 3D structures with the Au···Au (green–red dashed lines) internetwork interactions (the equivalent figures of **1·NO₂Bz** are at first glance indistinguible from those of **1·H₂O·MeOH**). (d) Perspective view of **1·H₂O·MeOH** showing the host–guest and guest–guest interactions between the water, methanol and the host framework.

accommodate the larger aromatic guest. Along the same lines, and as a consequence of the above mentioned Au1–N1–Fe1 angle differences, the acute Au···Fe···Au angle (ϕ) in the $\{Fe_4[Au(CN)_2]_4\}$ pseudo-square windows is slightly larger for **1·NO₂Bz** (78.8°, see Fig. 2c) than for **1·H₂O·MeOH** (71.6°). This effect is also related with the more regular arrangement of the network in **1·NO₂Bz** required to encapsulate the bulkier molecule of nitrobenzene. Similarly, the absence of disorder in the pyridine of **1·NO₂Bz** seems to be associated with the blocking action caused by the trapped nitrobenzene molecules. To estimate the amount of included nitrobenzene, an electron mask was applied in the structure of **1·NO₂Bz** determining the presence of 1 molecule of nitrobenzene per Fe^{II} ion, which is consistent with the TGA measurements (Fig. S1, ESI†).

When cooling to 120 K, the crystals change their colour to red, but maintaining both the orthorhombic *Cmma* space

group and the general structure described at 250/260 K. However, the observed $\langle Fe^{II}–N\rangle_{av}$ values are 1.955 Å (**1·NO₂Bz**) and 1.966 Å (**1·H₂O·MeOH**) which correspond well with that expected for the Fe^{II} in the LS state configuration and, therefore, indicate the occurrence complete HS-to-LS transitions. Furthermore, the aurophilic interactions become stronger [Au···Au = 3.064 (**1·NO₂Bz**) Å and 3.109 Å (**1·H₂O·MeOH**)] as well as the ϕ angles increase to 81.6 (**1·NO₂Bz**) and 75.2° (**1·H₂O·MeOH**).

Structure of 1·EtOH (monoclinic phase). At 200 K, the yellow crystals of **1·EtOH** display the monoclinic *P*2/*c* space group. As in the case of the orthorhombic **1·NO₂Bz** and **1·H₂O·MeOH** structures, the asymmetric unit consists in a unique pseudoocta-hedral [Fe^{II}N₆] site with four equatorial [Au(CN)₂]⁻ anions and two equivalent dpyan axial ligands with a $\langle Fe–N\rangle_{av}$ equal to 2.167 Å, indicating that the Fe^{II} ions present a HS configuration (Fig. 3a). However, in this case, there are two types of [Au(CN)₂]⁻

13908 | *J. Mater. Chem. C*, 2023, **11**, 13905–13916

This journal is © The Royal Society of Chemistry 2023

and the Au–N–Fe angles are considerably more deviated from linearity than those of the orthorhombic phase (Au1–N1-Fe1 = 147.32°, Au2–N2-Fe1 = 167.09°, Au2–N3-Fe1 = 146.37°, Au1–N4-Fe1 = 166.81°). Moreover, the monoclinic structure does not show positional disorder in any of the aromatic rings of the dpyan ligand and the NH$_2$ group is disordered only within two contiguous C of the central aniline ring (labelled as N7 and N8 with relative occupancies of 0.3 and 0.7, respectively). Although **1·EtOH** shows a double interpenetrated 3D structure similar to **1·NO$_2$Bz** and **1·H$_2$O·MeOH**, significant differences on the packing mode and shape of the network are observed. Indeed, even if, similarly than in the orthorhombic phase, the dpyan ligand of one network passes through the centroid of the Fe$_4$[Au(CN)$_2$] window of the other, this window is highly distorted and shows a marked rhomboidal shape [the acute Au···Fe···Au angle (ϕ) is 58.8°] (Fig. 3b). As a result of this window distortion, compound **1·EtOH** displays appreciably weaker internetwork aurophilic interactions (Au1···Au1 = 3.382 Å and Au2···Au2 = 3.348) but, in contrast, it promotes the presence of π···π interactions operating between adjacent dpyan ligands belonging to different networks (C···C distances between 3.5–3.8 Å, see Fig. S6 and Table S5, ESI†). In good accord with the TGA (Fig. S1, ESI†), 1.5 molecules of ethanol are located in two crystallographically independent sites, which have been unambiguously identified within the pores. These ethanol guests stablish multiple H-bonds through its OH groups with the NH$_2$ functions of the host framework attaching the guests in specific positions within the 1D cavities (Fig. 3c, Fig. S7 and Table S6, ESI†).

When cooling down to 120 K, the crystal of **1·EtOH**, which changes its colour to red, shows the same monoclinic $P2/c$ space group with a similar structure as that described at 200 K. However, the $\langle$Fe–N$\rangle_{av}$ (1.947 Å) is 0.220 Å shorter than at 200 K, reflecting a complete HS-to-LS transition upon cooling. Additionally, the aurophilic interactions become slightly shorter upon SCO (Au1···Au1 = 3.278 Å and Au2···Au2 = 3.234 Å) and the ϕ angle increases to 63.3°.

Powder X-ray diffraction (PXRD)

PXRD was carried out to verify the crystal phase purity of the bulk samples and to detect eventual crystallographic transformations accompanying the guest desorption processes. This technique has also been used to provide structural information for **1·MeOH** and **1·ø** whose structures could not be obtained through SCXRD.

The diffraction patterns of all samples were recorded for the air-dried crystalline powders and for their fully desolvated counterparts (Fig. 4 and Scheme 2). Moreover, the diffraction patterns of solvated samples (**1·MeOH**, **1·EtOH** and **1·H$_2$O·MeOH**) were also obtained whilst immersed in their mother liquor (ML) to avoid the loss of their volatile guests. Since the nitrobenzene molecules are not desorbed at room temperature, the compound **1·NO$_2$Bz** was directly analysed after being air-dried.

For **1·EtOH**, ML and air-dried diffractograms are very similar to that simulated from the SCXRD data. This observation reveals that both the as-synthesized and the air-dried crystals of **1·EtOH** display exclusively the same monoclinic phase described above for **1·EtOH**. Moreover, the diffraction pattern remains practically intact after heating the sample to fully desorb the ethanol molecules, indicating that the empty **1·ø** retains the monoclinic structure of its parent solvate **1·EtOH**
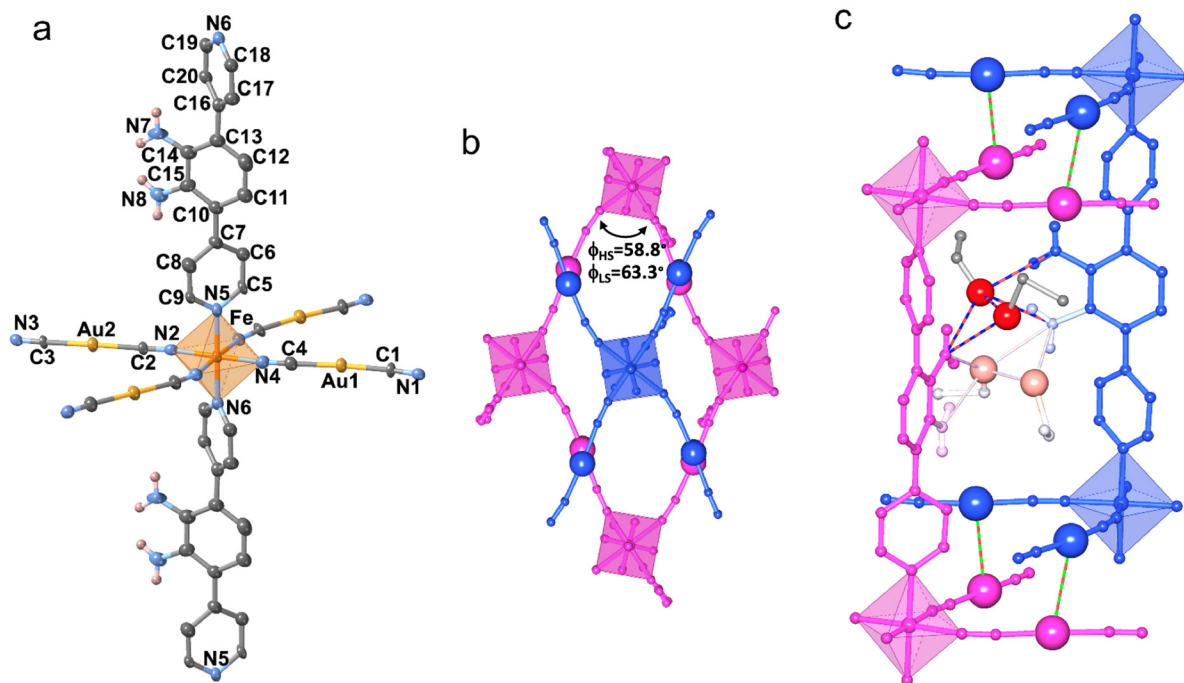
Fig. 3 (a) Octahedral environment of compound **1·EtOH** showing the atom labeling of the asymmetric unit. Corresponding (b) up and (c) side view of the interpenetration mode of **1·EtOH** displaying the ethanol molecules accommodated througout the 1D cavities. Green-red and blue-red dashed lines represent the host–host and host–guest interactions, respectively.

This journal is © The Royal Society of Chemistry 2023

J. Mater. Chem. C, 2023, 11, 13905–13916 | **13909**

Fig. 4 PXRD patterns of solvates **1**·**guest** [guest = MeOH and EtOH (a); NO$_2$Bz and H$_2$O·MeOH (b)] immersed in the mother liquor (ML), as air-dried samples and upon desolvation (or partial desolvation) after thermal treatment (**1**·**ø**). The simulated patterns (grey plots) of **1**·**EtOH** (a) and **1**·**H$_2$O**·**MeOH** and **1**·**NO$_2$Bz** (b) in the HS are also depicted for comparison. Orthorhombic and monocli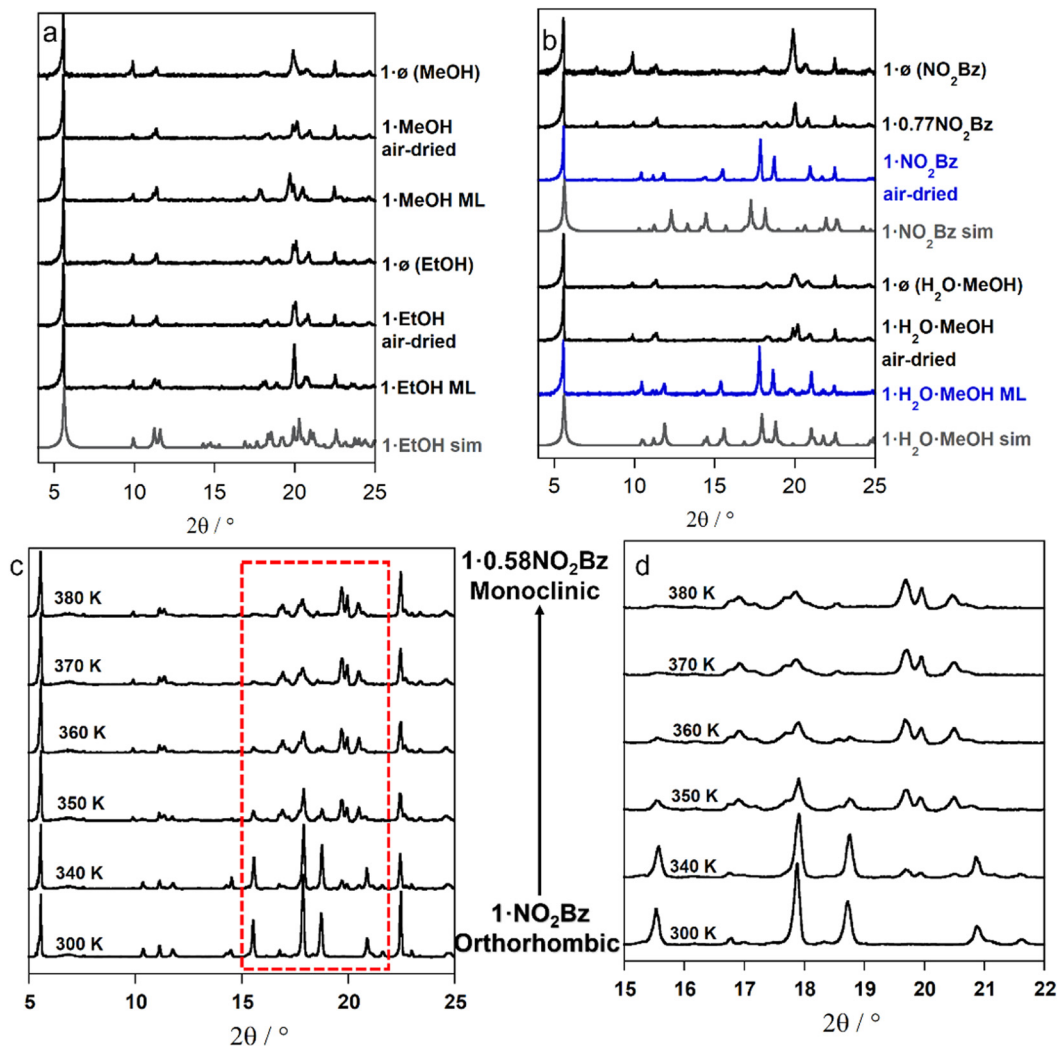nic phases are highlighted in black and blue plots, respectively. The solvent in parentheses indicates the parent solvate. (c) Evolution with temperature of the PXRD pattern of **1**·**NO$_2$Bz** and d) the corresponding enlarged 2θ range between 15 and 22°.
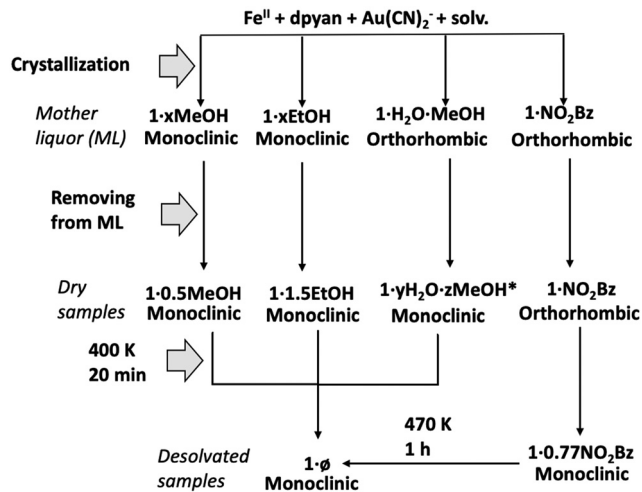
(Fig. 4a). A similar situation is observed for **1**·**MeOH** (Fig. 4a) whose ML and air-dried diffraction patterns are essentially the same and coincides with that of **1**·**EtOH**, demonstrating that both solvates are isostructural. Indeed, the same pattern can be obtained after heating either **1**·**EtOH** or **1**·**MeOH**, the latter merely producing a slightly less crystalline material.

Contrarily to **1**·**EtOH** and **1**·**MeOH**, compounds **1**·**H$_2$O**·**MeOH** and **1**·**NO$_2$Bz** exhibit important structural changes induced by the loss of guests (Fig. 4b). As expected, the diffraction patterns of **1**·**H$_2$O**·**MeOH** (ML) and **1**·**NO$_2$Bz** (air-dried) are similar and consistent with those simulated from the orthorhombic structures obtained through SCXRD. However, in the case of air-dried **1**·**H$_2$O**·**MeOH**, the spontaneous partial loss of solvent is accompanied by a drastic modification of the diffraction pattern from the orthorhombic to the monoclinic phase. The subsequent heating of the sample does not significantly modify the diffraction pattern and retains the monoclinic phase to yield **1**·**ø**.

Besides, when heating **1**·**NO$_2$Bz** at 400 K under air for 20 minutes, part of the nitrobenzene molecules desorbs yielding compound **1**·**0.77NO$_2$Bz**. The resulting diffraction pattern is that of the monoclinic phase showing that the slight loss of nitrobenzene provokes a crystal transformation from the orthorhombic to the monoclinic phase. Heating a fresh sample of **1**·**NO$_2$Bz** at 473 K under air for 1 h also yields the monoclinic compound **1**·**ø**.

Aiming at studying in detail this heating-induced orthorhombic→monoclinic phase change, we performed temperature-dependent *in situ* PXRD of **1**·**NO$_2$Bz**. Measurements were carried out under dynamic vacuum (see experimental details in ESI†) to obtain equivalent conditions to SQUID magnetometry (see below). As visible in Fig. 4c and d (enlarged scale), the orthorhombic diffraction pattern is maintained in the 300–340 K temperature range. In contrast, when heating above 340 K, a mixture of phases appears, showing an evolution from the orthorhombic to the monoclinic pattern. This phase change is completed within

13910 | *J. Mater. Chem. C*, 2023, **11**, 13905–13916

This journal is © The Royal Society of Chemistry 2023

Scheme 2 Synthesis, desolvation processes and crystallographic transformations of all solvates reported in this work. *According to TGA, y and z values are lower than 1.

370–380 K when the diffraction pattern of the pure monoclinic form is obtained. At this point, we determined the amount of retained nitrobenzene in this sample to be 0.58 molecules per Fe^{II} (Fig. S8, ESI†) *via ex situ* TGA. This confirms that the crystallographic phase change is coupled to the loss of guest which in turn is accelerated by vacuum.

Furthermore, it is worth noting that the transition from the orthorhombic to the monoclinic form, upon $1·H_2O·MeOH \rightarrow 1·ø$ and $1·NO_2Bz \rightarrow 1·ø$ transformations, is fully irreversible. Attempts of re-establishing the orthorhombic phase by immersing $1·ø$ in pure nitrobenzene or water/methanol solutions for a week did not recover the original orthorhombic form as the monoclinic phase was retained instead (Fig. S9, ESI†).

Spin crossover properties

Thermally induced spin crossover (SCO) properties were analysed for representative crystalline powder samples of the corresponding solvates. The SCO was studied with a SQUID magnetometer by measuring the $\chi_M T$ product at variable temperature with a scan rate of 2 K min^{-1} (χ_M is the molar magnetic susceptibility and T is the temperature. See the Experimental Section in the ESI† for more details). Given the lability of the guests in compounds $1·MeOH$, $1·EtOH$ and $1·H_2O·MeOH$ and aiming to investigate the guest effect on the SCO behaviour, the samples were measured first, in the ML, then, after air-dried and, finally, after desorbing the samples at 400 K. Due to the stability of the nitrobenzene guests in $1·NO_2Bz$ at room temperature, this sample was measured first in its air-dried state, later, partially desolvated at 400 K and finally fully desolvated at 473 K.

Magnetic properties of 1·MeOH and 1·EtOH. In the ML, both $1·MeOH$ and $1·EtOH$ exhibit a $\chi_M T \approx 3.2$ cm^3 K mol^{-1} at 280 K which is indicative that all the Fe^{II} ions are in the HS state (Fig. 5a and b, black curves). Upon cooling, this value remains constant until *ca.* 180 K for $1·MeOH$, to then drop abruptly down to 0.3 cm^3 K mol^{-1} at 120 K, a value assignable to the LS state. Upon heating, this latter $\chi_M T$ value is maintained until a
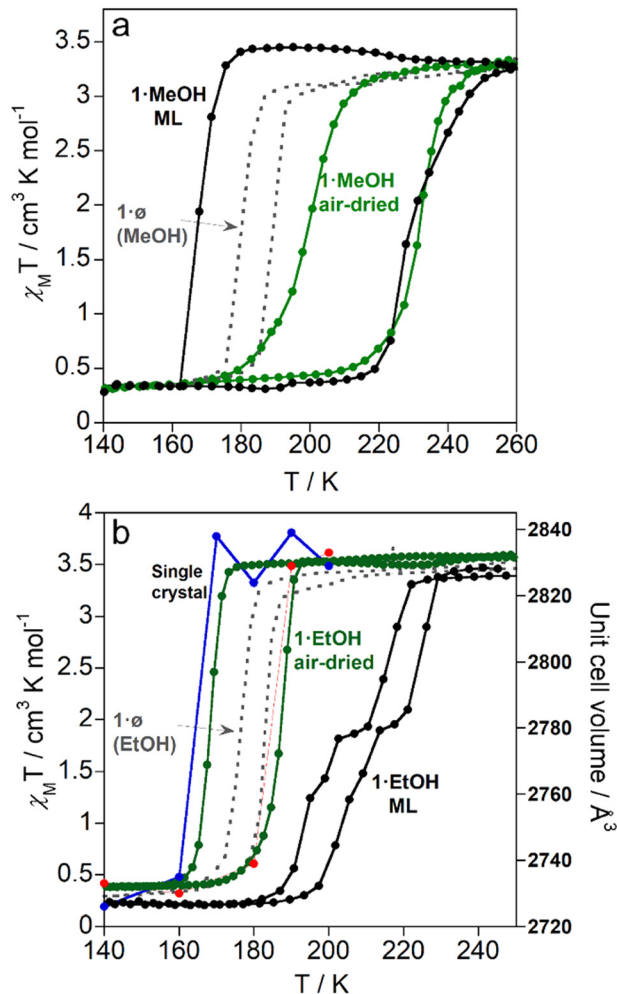

Fig. 5 $\chi_M T$ *vs.* T plots of compounds (a) **1·MeOH** and (b) **1·EtOH** measured in their ML (black plots), as air-dried samples (green plots) and after desolvation (dashed grey plots). The red (heating) and blue (cooling) plots in figure (b) represent thermal variation of the unit cell volume of a crystal of **1·EtOH**. The solvent in parentheses indicates the parent solvate.

temperature of *ca.* 220 K and then increases sharply to reach the initial value of 3.2 cm^3 K mol^{-1} at 260 K. The SCO equilibrium temperatures at which 50% of the Fe^{II} ions have changed its spin state during the cooling/heating mode, $T_{1/2}^\downarrow/T_{1/2}^\uparrow$, are 168.5/230 K. This magnetic behaviour indicates the occurrence of a complete spin transition with a very large hysteresis loop 61 K wide. In contrast, $1·EtOH$ exhibits a more moderate cooperative two-stepped spin transition characterized by a hysteresis width of 9 K [$T_{1/2}^{\downarrow 1}/T_{1/2}^{\uparrow 2}$/ = 216/225 K (first step) and $T_{1/2}^{\downarrow 2}/T_{1/2}^{\uparrow 1}$ = 196/205 K (second step)].

When the crystals of $1·MeOH$ and $1·EtOH$ are removed from the ML and dried under ambient conditions they give rise to the $\chi_M T$ *vs.* T plots displayed in Fig. 5a and b (green dotted lines). $1·MeOH$ undergoes a noticeable decrease of the hysteresis width from 61 K ($T_{1/2}^\downarrow = 169$ K, $T_{1/2}^\uparrow = 230$ K) to 32 K ($T_{1/2}^\downarrow = 200$ K, $T_{1/2}^\uparrow = 232$ K). Besides, the SCO behaviour of $1·EtOH$ displays a switch from two-step to a single-step SCO accompanied by an enlargement of the hysteresis loop from 9 to 19 K ($T_{1/2}^\downarrow = 168$ K, $T_{1/2}^\uparrow = 187$ K) and a decrease of $T_{1/2}$ by *ca.*

This journal is © The Royal Society of Chemistry 2023

J. Mater. Chem. C, 2023, **11**, 13905–13916 | **13911**

35 K. Interestingly, the measured thermal variation of the unit cell volume upon SCO of a single crystal of **1·EtOH**, is parallel to the corresponding $\chi_M T$ *vs. T* plot for the air-dried sample (see blue and red circles in Fig. 5b). This indicates that the measured crystal has already experienced partial ethanol desorption upon SCXRD measurement.

Finally, the SCO properties resulting from the fully desolvation of **1·MeOH** and **1·EtOH** [**1·ø**(MeOH) and **1·ø**(EtOH), respectively] are very similar. They exhibit complete spin transitions with $T_{1/2}^{\downarrow}/T_{1/2}^{\uparrow}$ equal to 180/189 K [**1·ø** (MeOH)] and 175/183 K [**1·ø** (EtOH)] featuring hysteresis widths of 9 and 8 K, respectively.

Magnetic properties of 1·H$_2$O·MeOH and 1·xNO$_2$Bz (x = 1, 0.77, 0.60, 0.34). As observed in Fig. 6a and b (black dotted lines), compounds **1·H$_2$O·MeOH** (ML) and **1·NO$_2$Bz** (air-dried) display, at 260 K, $\chi_M T$ values of *ca.* 3.2 cm K mol^{-1} consistent with the Fe^{II} ions presenting a HS state. Upon cooling, very similar decays of $\chi_M T$ with $T_{1/2}$ values around 205 K are observed unveiling gradual and complete spin transitions with very narrow hysteresis ($\Delta T < 2$ K). In order to assess if such SCO behaviour of the bulk sample is consistent with that of the individual single

crystals, the unit cell volume of **1·H$_2$O·MeOH** and **1·NO$_2$Bz** was also monitored as a function of temperature. As observed in Fig. 6a and b (blue and red dotted lines), the *V vs. T* curve fits well with the corresponding magnetic behaviour, thereby reflecting that the SCO of the isolated crystals is comparable with that of the bulk crystalline powder samples.

Once exposed to air, compound **1·H$_2$O·MeOH** experiences a partial solvent desorption concomitantly with an orthorhombic-to-monoclinic phase transformation as evidenced by TGA (Fig. S2, ESI†) and PRXD (Fig. 4b). As a result, the crystals of **1·H$_2$O·MeOH** undergo a marked increase of the hysteresis width up to 70 K ($T_{1/2}^{\downarrow} = 175$ K, $T_{1/2}^{\uparrow} = 245$ K, see grey dotted line curve in Fig. 6a). However, this large asymmetric hysteresis, recorded immediately after removing the crystals from the ML, is not stable over time and evolves to a less cooperative SCO behaviour at lower temperatures [*i.e.* $T_{1/2}^{\downarrow} = 152$ K/$T_{1/2}^{\uparrow} = 172$ K after 1 day (Fig. S10, ESI†) and $T_{1/2}^{\downarrow} = 150$ K/$T_{1/2}^{\uparrow} = 161$ K after 1 week (light grey dotted line in Fig. 6a)].

Ex situ thermal treatment at 400 K for 20 minutes of compound **1·NO$_2$Bz** triggers partial nitrobenzene desorption
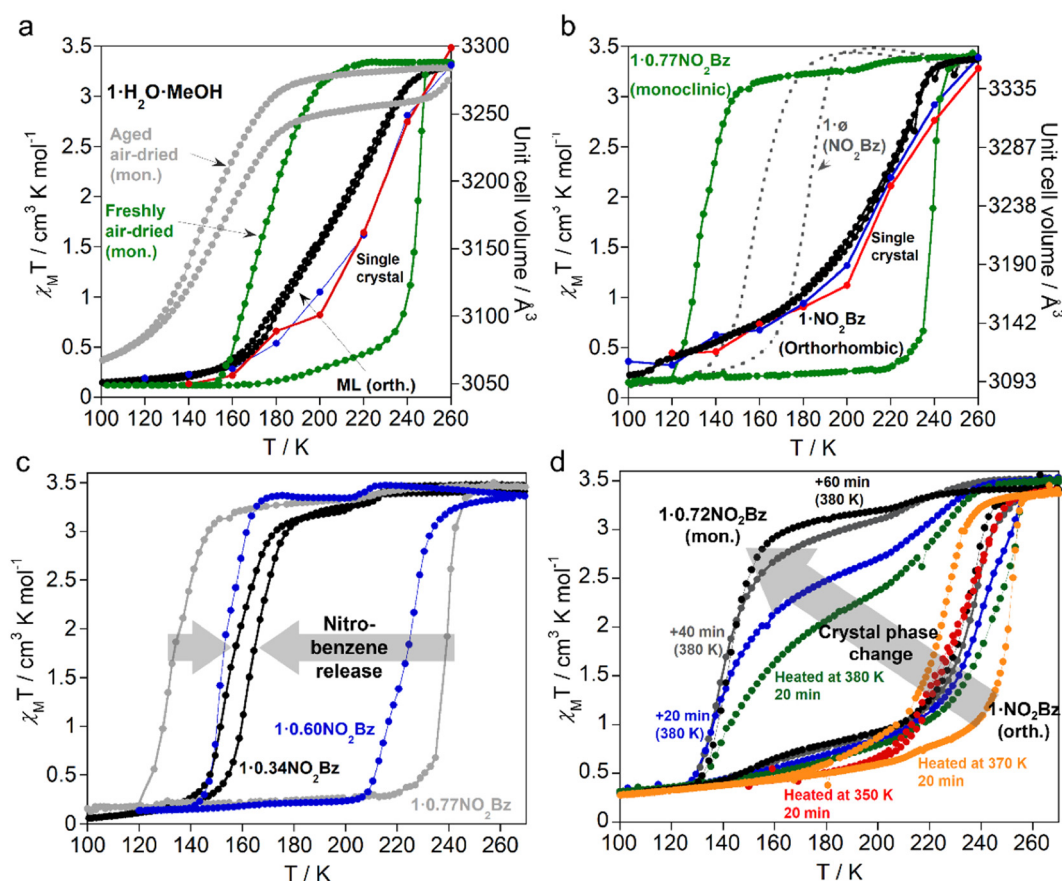

Fig. 6 (a) $\chi_M T$ *vs. T* plots of **1·H$_2$O·MeOH** measured in their ML (black plot) and as freshly (green plot)/aged (grey plot) air-dried samples. (b) $\chi_M T$ *vs. T* plots of **1·NO$_2$Bz** measured as air-dried sample (black plot) and upon removing partially (green plot) and completely (dashed grey plot) the nitrobenzene guest. (c) $\chi_M T$ *vs. T* behaviour of **1·xNO$_2$Bz** (monoclinic phase) with decreasing amounts of nitrobenzene. (d) Evolution of the $\chi_M T$ *vs. T* behaviour of a sample of **1·NO$_2$Bz** transforming from orthorhombic to monoclinic upon heating *in situ* within different thermal cycles. Note that in (a) and (b) compounds **1·H$_2$O·MeOH** and **1·NO$_2$Bz** change from the orthorhombic to the monoclinic phase when moving from the ML to the air-dried sample and from the air-dried sample to the desorbed sample, respectively. Figures (a) and (b) also depict the thermally induced unit cell volume change registered for the crystals of **1·H$_2$O·MeOH** and **1·NO$_2$Bz**, respectively (red and blue plots represent the cooling and heating modes).

13912 | *J. Mater. Chem. C*, 2023, **11**, 13905–13916

This journal is © The Royal Society of Chemistry 2023

($\mathbf{1 \cdot NO_2Bz} \rightarrow \mathbf{1 \cdot 0.77NO_2Bz}$) and concomitant orthorhombic-to-monoclinic crystallographic phase change (Fig. S3, ESI† and Fig. 4). Analogously to $\mathbf{1 \cdot H_2O \cdot MeOH}$, the crystallographic phase change involves the aperture of an outstanding thermal hysteresis (105 K, $T_{1/2}^{\downarrow} = 134$ K, $T_{1/2}^{\uparrow} = 240$ K) (Fig. 6b). However, due to the stability of the nitrobenzene guest in the structure, in this case, it is stable over time if stored at room temperature (Fig. S11, ESI†). Additionally, the cycle remains unaltered when measuring at different temperature scan rates (Fig. S12, ESI†). More vigorous *ex situ* thermal treatments and subsequent higher release of nitrobenzene provokes the narrowing of the hysteresis loop width which is 72 K for $\mathbf{1 \cdot 0.60NO_2Bz}$ ($T_{1/2}^{\downarrow} = 152$ K, $T_{1/2}^{\uparrow} = 224$ K, heating at 400 K for 120 min) and 8 K for $\mathbf{1 \cdot 0.32NO_2Bz}$ ($T_{1/2}^{\downarrow} = 155$ K, $T_{1/2}^{\uparrow} = 163$ K, heating at 400 K for 20 min) (Fig. 6c).

Aiming at recording the intermediate SCO behaviours evolving from the orthorhombic (gradual without hysteresis) to the monoclinic (cooperative with large hysteresis) forms, a fresh sample of $\mathbf{1 \cdot NO_2Bz}$ was progressively heated *in situ* in the SQUID chamber at increasing temperatures (350, 370 and 380 K) and subsequent $\chi_M T$ *vs.* T cycles from 100 to 270 K were recorded after each heating treatment. The results (Fig. 6d) indicate that while the magnetic behaviour is practically not changed upon heating at 350 K (red dotted line), the SCO is clearly modified after heating at 370 K (orange dotted line) opening a hysteresis up to 25 K wide with $T_{1/2}^{\downarrow} = 225$ K and $T_{1/2}^{\uparrow} = 250$ K. Further heating treatments at 280 K provokes a progressive widening of the hysteresis loop (up to 91 K; $T_{1/2}^{\downarrow} = 140$ K; $T_{1/2}^{\uparrow} = 231$ K) displaying in the cooling mode a gradual evolution from a double to a single step. The TGA carried out on the resulting solvate after the thermal treatments reveals the presence of 0.72 molecules of nitrobenzene (Fig. S13, ESI†).

Finally, the complete desorption of solvent in $\mathbf{1 \cdot H_2O \cdot MeOH}$ (20 min at 400 K) and $\mathbf{1 \cdot NO_2Bz}$ (1 h at 470 K) yields $\mathbf{1 \cdot \varnothing}$ ($H_2O \cdot$ MeOH) and $\mathbf{1 \cdot \varnothing}$ (NO_2Bz) which exhibit complete spin transitions with $T_{1/2}^{\downarrow}/T_{1/2}^{\uparrow}$ equal to 187/197 K (Fig. S12, ESI†) and 161/180 K (Fig. 6b) and hysteresis widths of 10 and 19 K, respectively.

Magnetic properties of the re-solvated species. The $\chi_M T$ *vs.* T curve of a sample of $\mathbf{1 \cdot \varnothing}$ exposed to air moisture for three days (recovering 0.7 molecules of water according to the TGA, Fig. S4, ESI†) was recorded. The results indicate that the re-adsorption of water shifts the SCO towards lower temperatures becoming more gradual with respect to the solvent free counterpart (Fig. S14, ESI†).

In order to prove the reversibility of the SCO properties throughout the $\mathbf{1 \cdot guest(as~synthesized)} \rightarrow \mathbf{1\varnothing} \rightarrow \mathbf{1 \cdot guest}$-(re-adsorbed) sequence, a sample of $\mathbf{1 \cdot \varnothing(MeOH)}$ was immersed in methanol, ethanol or nitrobenzene solutions and measured in suspension. Successive thermal cycles were carried out until stabilization of the SCO properties upon guest adsorption. In all cases, the resulting SCO behaviours are quite different to those of the as synthesized compounds (Fig. S15, ESI†). The $\chi_M T$ *vs.* T plots of the resolvated compounds $\mathbf{1 \cdot NO_2Bz}$ and $\mathbf{1 \cdot EtOH}$ display non-hysteretic gradual and incomplete spin transitions with $T_{1/2}$ values below that of the desolvated compounds [155 K ($\mathbf{1 \cdot NO2Bz}$); 172 K ($\mathbf{1 \cdot EtOH}$)]. In contrast, in the

case of $\mathbf{1 \cdot MeOH}$, the SCO shifts towards higher temperatures showing $T_{1/2}^{\downarrow}/T_{1/2}^{\uparrow}$ of 219 and 226 K and 5 K of hysteresis.

Discussion

In this work, we have explored the use of an amino functionalized organic ligand (dpyan) to assemble the 3D porous Hofmann-type Fe^{II}-based coordination polymer $\{Fe(dpyan)[Au(CN)_2]_2\} \cdot$guest ($\mathbf{1 \cdot guest}$), in order to combine synergistic host–guest and spin crossover properties. Depending on the solvent used during the synthesis, two types of polymorphic forms are predictably adopted by $\mathbf{1 \cdot guest}$. When the guest is nitrobenzene ($\mathbf{1 \cdot NO_2Bz}$) or water/methanol ($\mathbf{1 \cdot H_2O \cdot MeOH}$) we obtain an orthorhombic phase whereas when it is methanol ($\mathbf{1 \cdot MeOH}$) or ethanol ($\mathbf{1 \cdot EtOH}$) we observe a monoclinic structure. Although both polymorphs are characterized by a comparable double interpenetrated network, they present differences in the flexion degrees of the rhombic $\{Fe(Au(CN_2)_2\}$ grids which are more (monoclinic) or less (orthorhombic) distorted as a function of the nature of the trapped guest.

From a structural point of view, it seems that the stability of one polymorph *versus* the other is determined by the competition between the host–guest and host–host interactions. Thus, in the orthorhombic $\mathbf{1 \cdot NO_2Bz}$ and $\mathbf{1 \cdot H_2O \cdot MeOH}$ species, the interactions stablished between the disordered guests and the main network controls the stabilization of an orthorhombic high symmetry structure even if this conformation disables the establishment of significant host–host interactions other than the aurophilic ones. In contrast, in the monoclinic $\mathbf{1 \cdot MeOH}$ and $\mathbf{1 \cdot EtOH}$ compounds, the alcohol guests are highly oriented and occupy specific positions. These guest locations are compatible with the deformation and loss of symmetry of the framework which allows the attainment of concomitant host–guest and host–host $\pi \cdots \pi$ interactions together with the Au$\cdots$Au contacts. Although, the latter become significantly weaker. In the absence of guest ($\mathbf{1 \cdot \varnothing}$), the driving force of the structural conformation relays essentially in the host–host $\pi \cdots \pi$ interactions which lead to the monoclinic form. Importantly, the stabilization of the monoclinic phase is irreversible since the transformation back to the orthorhombic phase induced by the re-adsorption of nitrobenzene or water/methanol is not produced. It turns out that the energy required to revert the $\pi \cdots \pi$ interactions stablished between the interpenetrated networks in the monoclinic phase cannot be compensated by the entry of guest. The higher stability of the monoclinic *versus* the orthorhombic phase is also evidenced by the orthorhombic-to-monoclinic transformation observed for the as-synthesised $\mathbf{1 \cdot NO_2Bz}$ and $\mathbf{1 \cdot H_2O \cdot MeOH}$ upon the partial desorption (even a small amount) of guest.

The SCO properties exhibited by the solvates $\mathbf{1 \cdot guest}$ reflect a marked dependence on the nature of the adsorbed guest which is explained by the sensitivity that the $-NH_2$ confers to the host framework. However, while a clear guest-dependence of the SCO is observed for the monoclinic polymorph, the magneto-structural data reveals a poor SCO guest dependence for the

This journal is © The Royal Society of Chemistry 2023

J. Mater. Chem. C, 2023, **11**, 13905–13916 | **13913**

orthorhombic one. Indeed, the orthorhombic forms of **1·NO₂Bz** and **1·H₂O·MeOH** present very similar gradual SCO behaviours without meaningful modifications when passing from nitrobenzene to H₂O·MeOH (Fig. 6a and b, black curves). It appears that, in this case, the resulting SCO profiles are rather determined by the polymorph packing which lacks $\pi \cdots \pi$ interactions affording a bad communication between the Fe^{II} centres. Besides, the difference of size between nitrobenzene and water/methanol guests does not result in a substantial $T_{1/2}$ modification indicating the absence of significant steric effects.

In contrast, the guest induced wide range modulation of the SCO in the monoclinic polymorph is remarkable. The most notable example is indeed observed for **1·NO₂Bz**. When **1·NO₂Bz** is gently heated, a small fraction of nitrobenzene is released (**1·NO₂Bz → 1·0.77NO₂Bz**) and, concomitantly, the system undergoes a crystallographic change from the orthorhombic to the monoclinic phase. As a result, the SCO properties change drastically moving from a very gradual 2 K wide hysteresis to a cooperative 105 K wide hysteresis. This value is only 5 K narrower than that of $[Fe^{II}(1,2,3\text{-triazolate})_2]$[24] which exhibits, for the best of our knowledge, the widest hysteresis for a 3D SCO polymeric complex.

The suggested mechanism explaining the marked effect of the crystallographic phase change on the SCO properties is based on the intrinsic structural characteristics of the involved polymorphs and their respective interactions with the nitrobenzene guest. The exceptionally low $T_{1/2}^{\downarrow}$ value observed for the monoclinic **1·0.77NO₂Bz** compound can be attributable to steric factors which would gain importance with respect to that observed for the orthorhombic form. This, in turn, can be explained by the considerable decrease of the calculated accessible void space (in the HS state) when moving from the orthorhombic (868.0 Å^3) to the monoclinic (627.9 Å^3) phase. However, once the HS → LS transition has occurred, the LS state may be stabilized through electronic factors induced by directional H-bond interactions between the nitrobenzene guests and the NH₂ groups. This suggested mechanism for the occurrence of hysteresis is indeed consistent with the SCO behaviours observed after successive losses of nitrobenzene. Thus, when decreasing the amount of trapped nitrobenzene, both steric and electronic effects diminish yielding, as a result, hysteresis loops with increasing $T_{1/2}^{\downarrow}$ and decreasing $T_{1/2}^{\uparrow}$ and thereby with decreasing hysteresis widths. Similar conclusions of the source of bi-stability were reported by Konar *et al.* describing the increase of hysteresis width displayed by a 3D compound when substituting the guest molecules of acetonitrile by stilbene.[25]

Indeed, the same mechanism may explain the SCO behaviour observed for compound **1·H₂O·MeOH** and **1·MeOH**. The former exhibits a 70 K hysteresis wide appearing upon the orthorhombic-to-monoclinic crystallographic change. However, in this case, the hysteresis width decreases with time due to the progressive spontaneous loss of guest. The latter shows, in the mother liquor, a hysteresis 61 K wide which narrows to 32 K upon exposing to air, also prompted by a methanol loss. Thus, although **1·H₂O·MeOH** and **1·MeOH** exhibit SCO behaviours with analogue characteristics to that of **1·0.77NO₂Bz**, the higher volume and capacity to generate

host–guest interactions of nitrobenzene *versus* methanol or water account for the more pronounced bi-stability of the latter.

The ability of the desolvated compounds **1·ø** to readsorb guest molecules is manisfested in the modification of the SCO properties upon guest re-uptake (Fig. S15, ESI†). These guest re-adsorptions, performed by preparing a suspension of **1·ø** in the different solvents, do not culminate in the reestablishment of the SCO properties of the original as-synthesized samples. For example, the re-adsorption of nitrobenzene and ethanol leads to very gradual and incomplete spin transitions without hysteresis which contrast with the hysteretic and cooperative plots of the original **1·EtOH** and **1·0.77NO₂Bz** monoclinic compounds. This observation can be attributed to the mechanism of diffusion of the ethanol and nitrobenzene molecules into the host framework channels (Scheme 3). Due to the bulky volume of these guests, the diffusion may be slow filling and saturating the structural channels from the surface as the guest is being adsorbed. This guest saturation, which may hinder the SCO, is not produced in the genuine synthesis of the solvates which naturally crystallize with a homogeneous quantity of guest in the pores with a closed structure that avoids the entry of extra solvent.

Besides, whereas the re-adsorption of methanol increases notably the $T_{1/2}$ with respect to **1·ø**, it slightly decreases the cooperativity of the SCO while maintaining a hysteresis of 8 K. Similarly, the adsorption of water also decreases the cooperativity conserving a hysteresis of 8 K although at lower temperatures (Fig. S14, ESI†). Similar loss of cooperativity has been observed in related 2D Hofmann networks and explained by elastic frustration within the crystal lattice upon guest loading.[26,27] It turns out that, likely due to the lower volume of water and methanol, the steric effects are less marked than with ethanol and nitrobenzene and
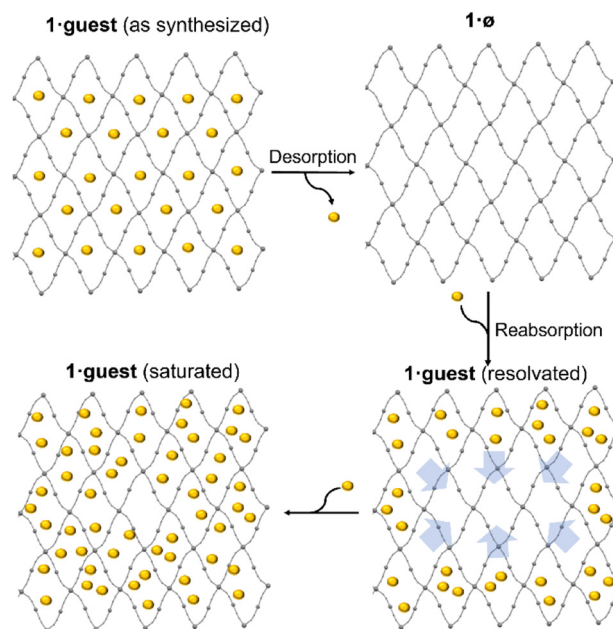
Scheme 3 Suggested mechanism for the desorption and re-adsorption of guest leading to saturated pores.

13914 | *J. Mater. Chem. C*, 2023, **11**, 13905–13916

This journal is © The Royal Society of Chemistry 2023

indeed, they are combined with electronic effects affecting notably to the spin crossover temperature. Further studies of the re-adsorption process with solvents of different nature, functional groups and size would be desirable to explore in detail the guest effect of the title compound.

Conclusions

In summary, we have investigated the dynamic host–guest interplay in a doubly interpenetrated porous 3D Hofmann-type coordination polymer functionalized with amino groups. The compound features a primitive cubic topology stemming from self-assembling the $[Au(CN)_2]^-$ and the 2,5-di(pyridin-4-yl)aniline (dpyan) bis-monodentate rod-like ligands around the Fe^{II} node. During the crystal growth, two different polymorphs have been isolated depending on the nature of the guests included in the pores: one orthorhombic and another monoclinic. The former, displaying a reasonably regular framework, is metastable and strongly distorts like a flexible wine rack structural motif, to give a denser structure in the monoclinic form. This irreversible transformation is essentially triggered by a threshold of spontaneous or induced removal of guests from the pores. Interestingly, this structural change involves a drastic modification of the SCO properties moving from gradual without hysteresis to cooperative with very large hysteresis spin transitions. We associate these dramatic SCO variations upon phase change to the increase of the guest induced steric effects and to an enhancement of the host–guest interactions delaying, respectively, the HS → LS and the LS → HS transitions, giving rise therefore to wide regions of bi-stability. Besides, the irreversibility of the orthorhombic to monoclinic transition nicely illustrates that, during the crystal growth, the guests act as templates to afford the metastable form. However, once in the monoclinic desolvated form, the distortion of the framework, stabilized by closer interactions between the interpenetrated frameworks, does not allow the solvents reverting the system to the orthorhombic form. Indeed, due to the inhomogeneous guest distribution, the SCO properties of the resulting re-solvated monoclinic are clearly different to the as-synthesized compounds. The results reported in this work give insight about reaching the optimal pathways for the design of SCO bi-stable PCPs.

Author contributions

Alejandro Orellana-Silla: investigation, methodology, writing – review & editing; Manuel Meneses-Sánchez: investigation, writing – review & editing; Rubén Turo-Cortés: investigation, methodology, writing review & editing; Víctor Rubio-Giménez: investigation, writing-review & editing; Giel Arnauts: investigation, writing – review & editing; M. Carmen Muñoz: supervision, writing – review & editing, funding acquisition; Rob Ameloot: supervision, writing – review & editing, funding acquisition Carlos Bartual-Murgui: supervision, writing, original draft, investigation; J. Antonio Real: funding acquisition, supervision, writing – review & editing.

Conflicts of interest

There are no conflicts to declare.

Acknowledgements

References

1 Spin crossover in transition metal compounds I-III, *Top. Curr. Chem.*, ed. P. Gütlich and G. Goodwin, 2004, vol. 233–235.

2 P. Gütlich, A. Hauser and H. Spiering, *Angew. Chem., Int. Ed. Eng.*, 1994, **33**, 2024–2054.

3 C. Lefter, V. Davesne, L. Salmon, G. Molnár, P. Demont, A. Rotaru, A. Bousseksou, C. Lefter, V. Davesne, L. Salmon, G. Molnár, P. Demont, A. Rotaru and A. Bousseksou, *Magnetochemistry*, 2016, **2**, 18.

4 S. Brooker, *Chem. Soc. Rev.*, 2015, **44**, 2880–2892.

5 O. Kahn and J. Martinez, *Science*, 1998, **279**, 44–48.

6 T. K. Ekanayaka, G. Hao, A. Mosey, A. S. Dale, X. Jiang, A. J. Yost, K. R. Sapkota, G. T. Wang, J. Zhang, A. T. N'Diaye, A. Marshall, R. Cheng, A. Naeemi, X. Xu and P. A. Dowben, *Magnetochemistry*, 2021, 7, 3, DOI: 10.3390/magneto chemistry7030037.

7 M. Mannini, F. Pineider, P. Sainctavit, C. Danieli, E. Otero, C. Sciancalepore, A. M. Talarico, M.-A. Arrio, A. Cornia, D. Gatteschi and R. Sessoli, *Nat. Mater.*, 2009, **8**(3), 194–197.

8 T. Miyamachi, M. Gruber, V. Davesne, M. Bowen, S. Boukari, L. Joly, F. Scheurer, G. Rogez, T. K. Yamada, P. Ohresser, E. Beaurepaire and W. Wulfhekel, *Nat. Commun.*, 2012, **3**, 938.

9 M. Piedrahita-Bello, L. Salmon, G. Molnar, P. Demont, B. Martin and A. Bousseksou, *J. Mater. Chem. C*, 2020, **8**, 6042–6051.

10 M. C. Muñoz and J. A. Real, *Coord. Chem. Rev.*, 2011, **255**, 2068–2093.

11 W. Liu, Y.-Y. Peng, S.-G. Wu, Y.-C. Chen, M. N. Hoque, Z.-P. Ni, X.-M. Chen and M.-L. Tong, *Angew. Chem., Int. Ed.*, 2017, **56**, 14982–14986.

12 K. Yoshida, D. Akahoshi, T. Kawasaki, T. Saito and T. Kitazawa, *Polyhedron*, 2013, **66**, 252–256.

13 J. E. Clements, J. R. Price, S. M. Neville and C. J. Kepert, *Angew. Chem., Int. Ed.*, 2016, **55**, 15105–15109.

14 J.-Y. Li, Z. Yan, Z.-P. Ni, Z.-M. Zhang, Y.-C. Chen, W. Liu and M.-L. Tong, *Inorg. Chem.*, 2014, **53**, 4039–4046.

This journal is © The Royal Society of Chemistry 2023

J. Mater. Chem. C, 2023, **11**, 13905–13916 | **13915**

15 J.-Y. Li, C.-T. He, Y.-C. Chen, Z.-M. Zhang, W. Liu, Z.-P. Ni and M.-L. Tong, *J. Mater. Chem. C*, 2015, **3**, 7830–7835.

16 J. Y. Li, Y. C. Chen, Z. M. Zhang, W. Liu, Z. P. Ni and M. L. Tong, *Chem. – Eur. J.*, 2015, **21**, 1645–1651.

17 A. Martinez-Martinez, E. Resines-Urien, N. S. Settineri, S. J. Teat, E. C. Sañudo, O. Fabelo, J. A. Rodriguez-Velamazan, L. Piñeiro-López and J. S. Costa, *Cryst. Growth Des.*, 2023, **23**(6), 3952–3957.

18 Z.-P. Ni, J.-L. Liu, M. N. Hoque, W. Liu, J.-Y. Li, Y.-C. Chen and M.-L. Tong, *Coord. Chem. Rev.*, 2017, **335**, 28–43.

19 R. Ohtani and S. Hayami, *Chem. – Eur. J.*, 2017, **23**(10), 2236–2248.

20 M. Nakaya, R. Ohtani and S. Hayami, *Eur. J. Inorg. Chem.*, 2020, (39), 3709–3719.

21 Y. Xie, R.-B. Lin and B. Chen, *Adv. Sci.*, 2022, **9**(1), 2104234.

22 E. Resines-Urien, E. Fernandez-Bartolome, A. Martinez-Martinez, A. Gamonal, L. Piñeiro-López and J. S. Costa, *Chem. Soc. Rev.*, 2023, **52**(2), 705–727.

23 J. Tao, R. J. Wei, R. Bin Huang and L. S. Zheng, *Chem. Soc. Rev.*, 2012, **41**, 703–737.

24 M. Grzywa, R. Röb-Ohlenroth, C. Muschielok, H. Oberhofer, A. Błachowski, J. Żukrowski, D. Vieweg, H.-A. K. von Nidda and D. Volkmer, *Inorg. Chem.*, 2020, **59**, 10501–10511.

25 D. J. Mondal, B. Kumar, A. Paul and S. Konar, *J. Mater. Chem. C*, 2023, **11**, 6750–6759.

26 K. A. Zenere, S. G. Duyker, E. Trzop, E. Collet, B. Chan, P. W. Doheny, C. J. Kepert and S. M. Neville, *Chem. Sci.*, 2018, **9**, 5623–5629.

27 D. J. Mondal, A. Mondal, A. Paul and S. Konar, *Inorg. Chem.*, 2022, **61**, 4572–4580.

13916 | *J. Mater. Chem. C*, 2023, **11**, 13905–13916

This journal is © The Royal Society of Chemistry 2023